Stochastic sensitivity analysis of the noise-induced excitability in a model of a hair bundle

Irina Bashkirtseva,[1,*] Alexander B. Neiman,[2,†] and Lev Ryashko[1,‡]
[1]*Department of Mathematics, Ural Federal University, Pr. Lenina 51, Ekaterinburg, Russia*
[2]*Department of Physics and Astronomy, Ohio University, Athens, Ohio 45701, USA*
(Received 17 January 2013; published 17 May 2013)

We study effect of weak noise on the dynamics of a hair bundle model near the excitability threshold and near a subcritical Hopf bifurcation. We analyze numerically noise-induced structural changes in the probability density and the power spectral density of the model. In particular, we show that weak noise can induce oscillations with two distinct frequencies in both excitable and limit-cycle regimes. We then applied a recently developed technique of stochastic sensitivity functions which allows us to estimate threshold values of noise intensity corresponding to these transitions.

DOI: 10.1103/PhysRevE.87.052711 PACS number(s): 87.19.ln, 87.19.lo, 05.40.−a

I. INTRODUCTION

The interplay between stochasticity and nonlinearity in dynamical systems can generate various phenomena which are not observed in noise-free cases [1,2]. New stochastic regimes such as noise-induced transitions [3,4], stochastic bifurcations [5–7], stochastic resonance [8–10], noise-induced chaos [11–13], noise-induced excitability [14,15] and intermittency [16–18], and coherence resonance [19–23] are still the subject of intensive investigations.

Even weak noise can essentially deform the dynamics of a nonlinear system due to nonuniformity of its states in phase space. Usually such nonuniformity is associated with the multistability of the deterministic system. Indeed, Gaussian noise leads to global stability of a multistable system [24]; i.e., random phase trajectories eventually surmount separatrix barriers separating basins of the attraction of coexisting states. However, in realistic settings the observation time is fixed or noise is bounded [25], which naturally leads to a threshold value of noise strength. As the noise intensity exceeds this threshold value, phase trajectories cross a separatrix and a new dynamical regime is established [26]. The threshold value of noise strength is determined by both the geometry of the basins of attraction and the sensitivity of states to random perturbations. Indeed, multistability is not the only condition for noise-induced changes in dynamics to occur. Excitable systems with a single attractor, e.g., stable equilibrium, exhibit noise-induced large-magnitude excursions [14]. For small perturbations the deterministic excitable system quickly relaxes back to the stable equilibrium. Once the deviation from the equilibrium reaches a certain threshold, a large excursion is observed. Here, the zones of different types of dynamics in phase space are separated by some curve "pseudoseparatrix" [27]. In such systems, weak noise causes small-amplitude stochastic oscillations around the deterministic equilibrium. As the noise intensity increases, the system demonstrates an abrupt rise of the amplitude of oscillations and a change of the dominating frequency [28,29]. Furthermore, the coherence of noise-induced oscillations can be maximized at an optimal noise level via the phenomenon of coherence resonance [19].

The challenge is to calculate the threshold noise strength at which a qualitative change in the dynamics occurs. Direct numerical simulations of random trajectories become cumbersome in the weak-noise limit. Therefore, asymptotic methods and approximations are commonly used for corresponding Fokker-Planck equations [30–32]. For example, approaches to the asymptotic probabilistic analysis of mixed-mode oscillations for slow-fast dynamical systems have been developed in [27,33].

Recently, a method for obtaining a statistical description of stochastic attractors has been developed. This method is based on the quasipotential theory [34,35], and it allows calculation of the so-called stochastic sensitivity function (SSF) [36,37] for the probabilistic description of stochastic attractors. Using SSF one can construct confidence domains (ellipses, bands, etc.) that adequately reflect the main features of the spatial arrangement of random states for small noise.

The SSF technique has been successfully applied to the analysis of backward stochastic bifurcations [38], noise-induced phenomena in the FitzHugh-Nagumo model [39], and noise-induced chaotic oscillations [40]. In the present study we extend the SSF method to the case of subcritical Andronov-Hopf (AH) bifurcation in which a noise-free system possesses coexisting stable equilibrium and stable limit cycle. Recently, several works were devoted to noisy subcritical AH bifurcation, e.g., in nonlinear optics [23] and in the Hodgkin-Huxley neuron model [41]. Our approach provides a statistical measure to assess directly and theoretically, i.e., without numerical simulations of stochastic equations, the critical noise intensities resulting in qualitative changes of the system's dynamics. To be specific, we investigate noise-induced effects in a realistic biophysical model of ciliary bundles of sensory hair cells near a subcritical Andronov-Hopf (AH) bifurcation and clarify a mechanism of interplay of stochasticity and geometrical arrangement of the phase trajectories using the SSF technique. We first introduce the model and show noise-induced bifurcations in an excitable regime and in a regime of coexistence of stable equilibrium and limit cycle using direct numerical simulations. Next we analyze the stochastic dynamics with the aid of the SSF technique and statistical confidence domains and provide

*irina.bashkirtseva@usu.ru
†neimana@ohio.edu
‡lev.ryashko@usu.ru

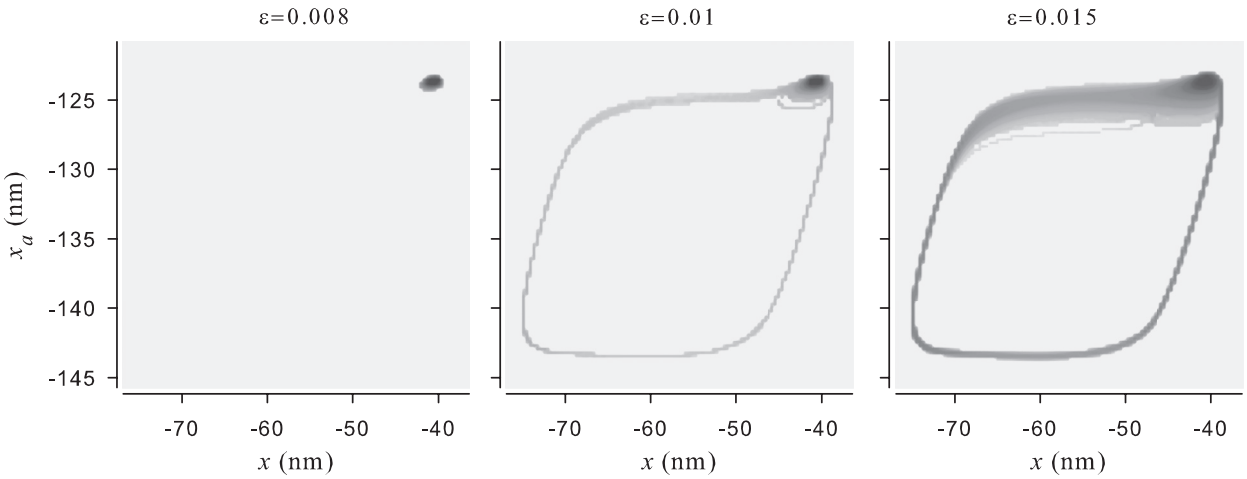

FIG. 1. Contour lines of the probability density function in the excitable regime for the indicated values of noise parameter ε. The parameters are $F_{\max} = 50.3$ pN and $S = 0.6212$.

theoretical estimates of threshold noise intensity leading to noise-induced bifurcations.

II. STOCHASTIC HAIR BUNDLE MODEL

We used a biophysical model developed in [42] to describe spontaneous mechanical oscillations of hair bundles in bullfrog saccular hair cells. Sensory hair cells are the first stage in conveying the mechanical stimuli into the electrical signals. The hair bundle is a bunch of 10–100 stereocilia emanating from the apical membrane of a hair cell. A hair cell converts deflection of the attached hair bundle into changes of the membrane potential using the mechanically gated ion channels on stereocilia. In the model the hair bundle is represented by a single structure subjected to three types of force: elastic forces, forces due to mechanoelectrical transduction ion channels, and forces due to myosin molecular motors, resulting in adaptation of the bundle to external forces. The state variables are the position of the bundle tip, x, and the position of the molecular motors, x_a, along the hair hair bundle axis projected to x. The hair bundle is subjected to random forces mimicking thermal Brownian motion of the bundle in viscous endolymph, stochastic cluttering of MET channels, and fluctuating forces on molecular motors [42]. The model's equations are

$$\begin{aligned} \lambda\dot{x} &= -K_{\mathrm{GS}}[x - x_a - DP_o(x,x_a)] - K_{\mathrm{SP}}x + \varepsilon\sqrt{2k_B\lambda T}\,\xi(t), \\ \lambda_a\dot{x_a} &= K_{\mathrm{GS}}[x - x_a - DP_o(x,x_a)] - F_{\max}(1 - SP_o) \\ &\quad + \varepsilon\sqrt{2k_B\lambda_a T_a}\,\xi_a(t), \end{aligned} \tag{1}$$

where λ and λ_a are the effective friction coefficients for the hair bundle and molecular motors, respectively, K_{GS} is an effective spring constant of gating links connecting stereocilia, K_{SP} is the stiffness of stereocilia pivots, and D is the gating swing of the MET channels. In Eq. (1) $P_o(x,x_a)$ is the open probability of MET channels given by

$$\begin{aligned} P_o(x,x_a) &= \frac{1}{1 + A\,e^{-(x-x_a)K_{\mathrm{GS}}D/(N_{\mathrm{GS}}k_BT)}}, \\ A &= e^{[\Delta G + K_{\mathrm{GS}}D^2/(2N_{\mathrm{GS}})]/(k_BT)}, \end{aligned} \tag{2}$$

where N_{GS} is the number of MET channels, k_B is the Boltzmann constant, T is the absolute temperature, and $\Delta G = 10\,k_BT$ [42]. In Eq. (1) $\xi(t)$ and $\xi_a(t)$ are uncorrelated white Gaussian zero-mean noise terms describing fluctuating forces on the hair bundle, $\xi(t)$, and on the molecular motors, $\xi_a(t)$. The control parameters of the deterministic model are the calcium feedback strength, S, and the maximal force of molecular motors, $F_{\max}$. To study the influence of noise we introduced another control parameter, ε, which was used to reduce the strength of thermal noise. We note that the intensity of noise in the model (1) is effectively reduced, e.g., in hair bundles coupled by elastic springs [43–45]. The values of other parameters used in the numerical simulations were [42,46] as follows: $\lambda = 2.8$ μN s/m, $\lambda_a = 10$ μN s/m, $K_{\mathrm{GS}} = 0.75$ mN/m, $K_{\mathrm{SP}} = 0.6$ mN/m, $D = 60.9$ nm, $N_{\mathrm{GS}} = 50$, $T = 300$ K, and $T_a = 450$ K. We used a Runge-Kutta method to integrate stochastic differential equations of the model (1) with the fixed time step $\Delta t = 10^{-5}$ s.

III. NOISE EFFECTS NEAR THE SUBCRITICAL ANDRONOV-HOPF BIFURCATION

In the absence of noise, $\varepsilon = 0$, the model demonstrates two types of attractor: equilibrium and limit cycle. In the parameter

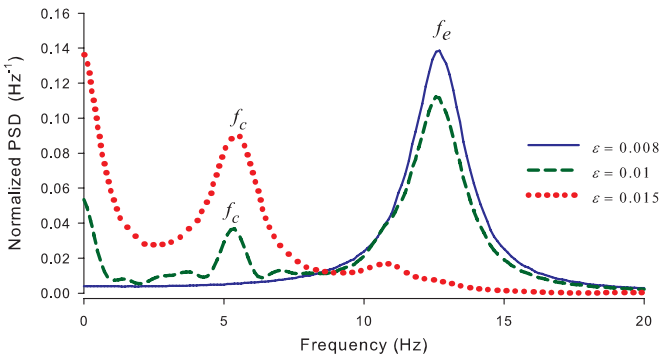

FIG. 2. (Color online) Power spectral density of $x(t)$ normalized to the variance of x for the same data as in Fig. 1. Frequencies of small-amplitude fluctuations around the stable equilibrium and of large-amplitude noise-induced excursions are indicated by f_e and f_c, respectively.

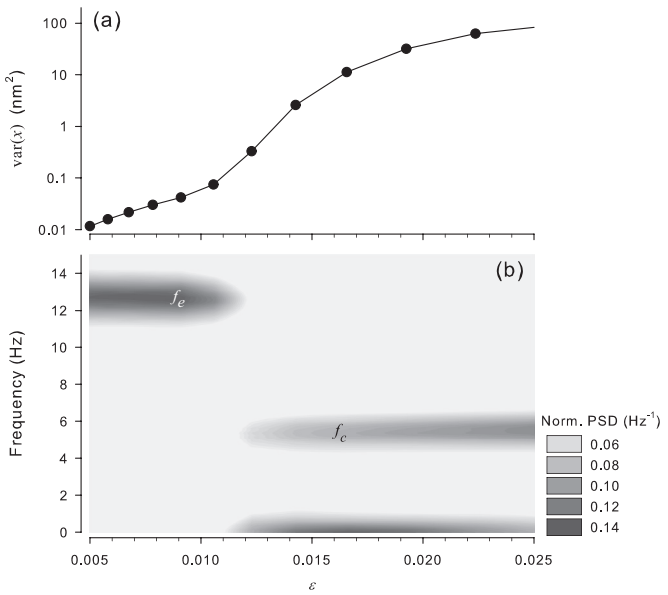

FIG. 3. Noise effect on the excitable regime. (a) Variance of $x(t)$, var(x), vs noise strength, ε. (b) Contour lines of the normalized PSD plotted for the same values of ε as in panel (a). Frequencies of small-amplitude fluctuations around the stable equilibrium and of large-amplitude noise-induced excursions are indicated by f_e and f_c, respectively. Other parameters are the same as in Fig. 2.

plane (S, $F_{\max}$) these regimes are separated by a curve of the Andronov-Hopf (AH) bifurcation [42,46]. In the following, we concentrate on the parameter region close to a *subcritical* AH bifurcation. In particular, we fix $F_{\max} = 50.3$ pN and vary the parameter S. For $0.6 < S < S_1 = 0.621269$, the deterministic system exhibits a stable equilibrium $(\bar{x},\bar{x}_a)$ only and is excitable. At $S = S_1$, a stable limit cycle is born through a saddle-node bifurcation. In the parameter range $S_1 < S < S_2 = 0.6223$ the model is bistable, possessing a stable equilibrium and stable limit cycle separated by a saddle limit cycle. At $S = S_2$ the saddle limit cycle merges with the equilibrium through the subcritical AH bifurcation and for $S > S_2$ the model has an unstable equilibrium and a stable limit cycle. In the following sections we use direct numerical simulations to show the noise effect near the subcritical AH bifurcation in the excitable regime (in which a stable equilibrium is the only attractor) and in the bistable regime (in which a stable equilibrium and a stable limit cycle coexist).

A. Excitable regime

We first analyzed the influence of weak noise on the excitable regime for $S = 0.6212 < S_1$. We set the integration time to be extremely large (5×10^4 s) to observe escape from small-amplitude fluctuations around the equilibrium to large-amplitude excitations. For $\varepsilon \leqslant 0.01$ these excursions were very rare so that the phase trajectories of the stochastic system spent most of their time in a small region around the equilibrium, as indicated in Fig. 1 (first two panels). For $\varepsilon \geqslant 0.015$ the system showed large excursions but returned and fluctuated around the stable equilibrium, as indicated by the high probability around the equilibrium in Fig. 1 (third panel).

It is instructive to analyze this behavior further with the aid of the power spectral density (PSD) of $x(t)$. In order to compare the frequency content of small fluctuations and large-amplitude excitations we normalized the PSD to the variance of $x(t)$. Figure 2 shows the PSDs of the model for the same noise amplitudes as in the previous figure for the probability densities. For $\varepsilon < 0.01$ the bundle fluctuated around the stable equilibrium and its PSD shows a single peak at $f_e = 12.69$ Hz, corresponding to the imaginary part of the equilibrium's eigenvalues. In this regime the system can be viewed as a noise-perturbed linear damped oscillator. At $\varepsilon = 0.01$ large excursions began to appear; these resemble a limit cycle which was about to be born if the parameter S were to increase. Notice that the frequency of large-amplitude stochastic excursions, $f_c = 5.61$ Hz, is lower than the frequency of small fluctuations around the equilibrium, f_e, indicated by the smaller amplitude peak in the PSD (green dashed line in Fig. 2). In this regime the dynamics of the hair bundle was biperiodic; i.e., the PSD contained two peaks, f_e and f_c. Importantly, the peak at f_e (equilibrium fluctuations) became wider, indicating that

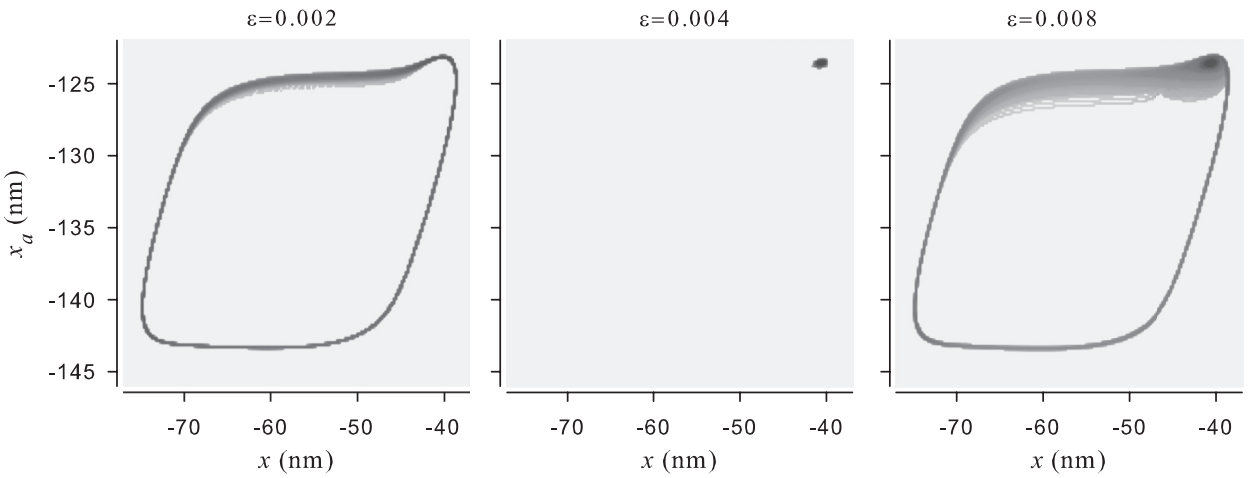

FIG. 4. Contour lines of the probability density function in the bistable regime for the indicated values of noise parameter ε. The parameters are $F_{\max} = 50.3$ pN and $S = 0.622$.

large-amplitude excursions destroyed the coherence of small-amplitude stochastic oscillations around the equilibrium. Furthermore, a peak at zero frequency indicated intermittency between small-amplitude fluctuations and large excursions. Thus, the structure of the PSD reflects the highly nonuniform motion of the hair bundle with long segments of fluctuations around the equilibrium interrupted by large-amplitude excitations. With further increase of noise large stochastic oscillations become dominant, as the PSD peaked at f_c, while the peak at f_e vanished (red dotted line in Fig. 2). However, the zero-frequency peak indicates that the system spent considerable time in the vicinity of the equilibrium (compare with the probability density in the third panel of Fig. 1).

These results are summarized in Fig. 3, which clearly shows the existence of a critical noise strength at $\varepsilon \approx 0.01$. First, the variance of the hair bundle position, var(x), shows two qualitatively different growth laws as the noise strength increases [Fig. 3(a)]. For $\varepsilon < 0.01$ the variance grows linearly with ε^2 as for a linear system perturbed by noise. This linear dependence is broken for larger noise, $\varepsilon > 0.01$, when large-amplitude excitations become more frequent. Second, this tendency is reflected in the PSD shown in Fig. 3(b): a linear response to noise is characterized by a single peak in the PSD at $f = f_e$. Noise-induced large-amplitude excitations result in the appearance of a lower frequency peak at $f = f_c$ and a zero-frequency peak due to intermittency between two types of motion. As noise continued to increase, the zero-frequency peak became smaller while the peak at f_c grew, reflecting that the residence of phase trajectories around the equilibrium became shorter and more power was concentrated around f_c. This last effect of enhanced oscillatory coherence due to noise abolishing the nonuniformity of motion is indeed well known [47].

B. Bistability of equilibrium and limit cycle

Similar numerical procedures were used for the bistability region, $S = 0.622$. We took initial conditions at the stable deterministic limit cycle. For small noise, $\varepsilon < 0.003$, the phase trajectories are weakly spread near the deterministic limit

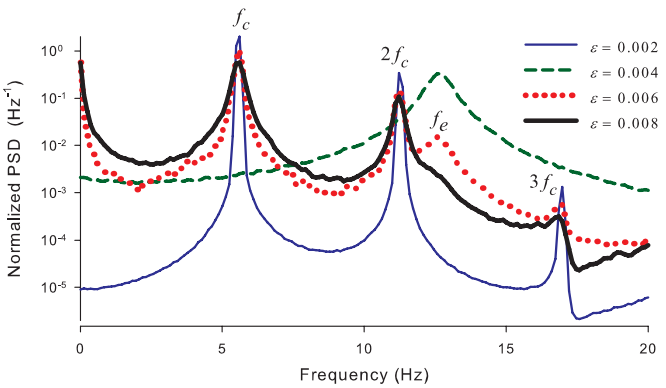

FIG. 5. (Color online) Power spectral density of $x(t)$ normalized to the variance of x for the same data as in Fig. 4. Frequencies of small-amplitude fluctuations around the stable equilibrium and of large-amplitude limit-cycle oscillations are indicated by f_e and f_c, respectively.

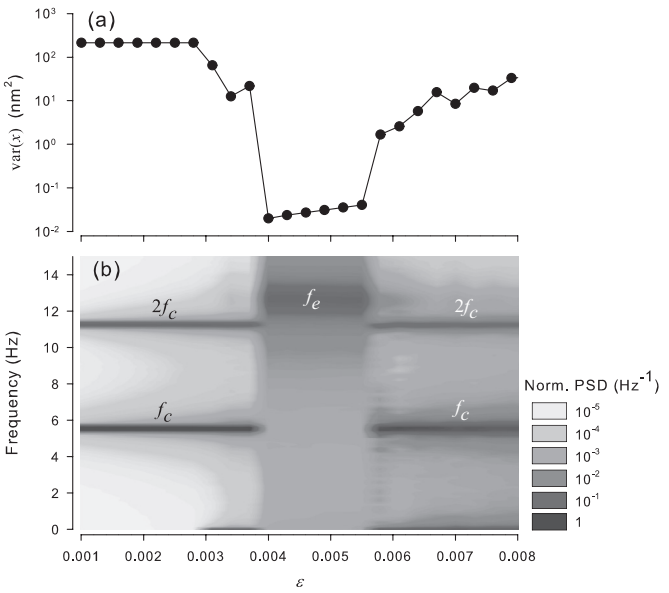

FIG. 6. Noise effect on the bistable regime. (a) Variance of $x(t)$, var(x), vs noise strength ε. (b) Contour lines of the normalized PSD plotted for the same values of ε as in (a). Frequencies of small-amplitude fluctuations around the stable equilibrium and of large-amplitude limit-cycle oscillations are indicated by f_e and f_c, respectively. Other parameters are the same as in Fig. 4.

cycle, as shown in Fig. 4 (left panel). The integration time of 5×10^3 s was not long enough for the system to surmount a barrier set by the unstable limit cycle separating stable attractors in phase space. However, a small increase of noise intensity resulted in escape to the basin of attraction of stable equilibrium. The integration time of 5×10^3 s was not long enough for the system to escape back to the limit cycle. As a result, the probability density peaked at the stable equilibrium, as Fig. 4 (middle panel) indicates. Further increase of noise results in hopping between the equilibrium and the limit cycle shown in Fig. 4 (right panel).

The PSD shown in Fig. 5 reflects this transition. For $\varepsilon < 0.003$ the PSD shows sharp peaks at the fundamental frequency of the limit cycle, f_c, and its higher harmonics (blue thin solid line in Fig. 5). After noise-induced escape to the equilibrium, $\varepsilon \approx 0.004$, the PSD peaked at a higher frequency

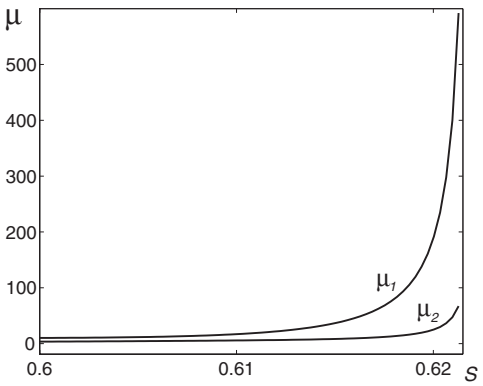

FIG. 7. Eigenvalues μ_1 and μ_2 of the stochastic sensitivity matrix for the stable equilibrium vs the parameter S.

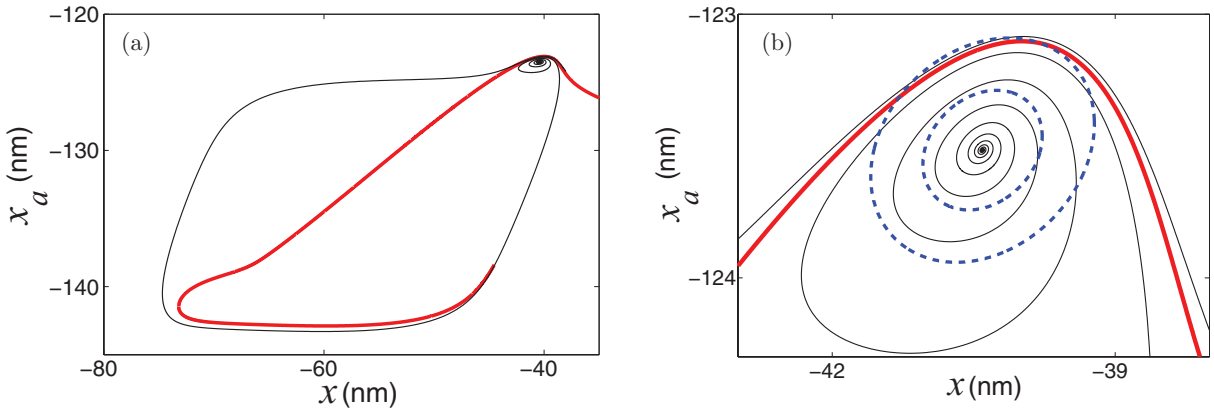

FIG. 8. (Color online) Phase portrait of the deterministic system and confidence ellipses. The deterministic phase trajectory is shown by the black thin line. The pseudoseparatrix is shown by the red thick line. Panel (b), an expansion of (a), also shows confidence ellipses (blue dashed lines) for $\varepsilon = 0.008$ (small) and $\varepsilon = 0.015$ (large) and for the fiducial probability $p = 0.999$. Other parameters are $F_{\max} = 50.3$ pN and $S = 0.6212$.

f_e, corresponding to noise-sustained small-amplitude oscillations around the equilibrium (green dashed line in Fig. 5). The peak frequency, f_e, and the width of the peak were mainly determined by the eigenvalues of the equilibrium. With further increase of noise the phase trajectories began hopping between the two attractors, expressing their fundamental frequencies in the PSD (red dotted line in Fig. 5). Note again a peak at zero frequency due to hopping dynamics. Finally, Fig. 6 summarizes the effect of noise on the bistable regime near the subcritical AH bifurcation. The variance of limit-cycle oscillations depended weakly on the noise intensity until ε reached its critical values at approximately 0.004 [Fig. 6(a)]. The phase trajectories residing in the basin of attraction of the stable equilibrium were characterized by a small variance and a wide peak at $f = f_c$ in the PSD [Fig. 6(b)]. For $\varepsilon > 0.005$ the dynamics was intermittent with phase trajectories residing in both attractors and performing rare transitions between them.

IV. ANALYSIS OF NOISE EFFECTS USING THE STOCHASTIC SENSITIVITY FUNCTION

In this section we use the stochastic sensitivity function technique to calculate the confidence domains for random trajectories to remain in a certain region in phase space and to estimate the threshold noise intensity for noise-induced bifurcations described in the previous section. Random phase trajectories remain within these domains with a prescribed fiducial probability. We stress again that the SSF technique does not require numerical simulation of stochastic trajectories. Instead it relies on stochastic sensitivity of a system to small random perturbations. The last property is quantified by the SSF function (see the Appendix). The construction of the confidence domain allows us to set up a straightforward criterion for the threshold noise intensity: an intersection of the confidence domains with a separatrix of the deterministic system provides the condition for noise-induced bifurcation.

A. SSF analysis of excitability

We start with the excitable regime where a stable equilibrium is the only attractor. Under random disturbances the trajectories of the system (1) leave the deterministic equilibrium and form a stochastic cloud around it. For small noise the dispersion of this cloud increases as the parameter S tends to the bifurcation value S_2. This expansion is explained

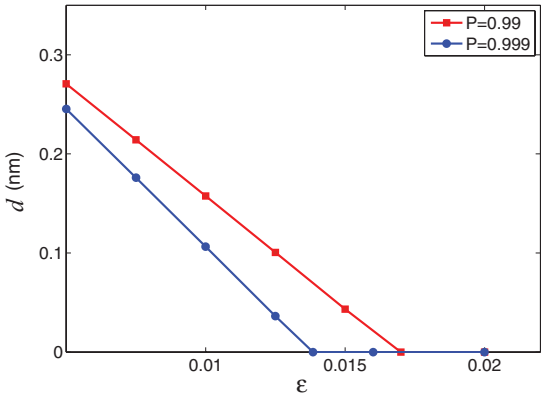

FIG. 9. (Color online) The distance between confidence ellipses and the pseudoseparatrix for $p = 0.99$ (red line with squares) and $p = 0.999$ (blue line with circles).

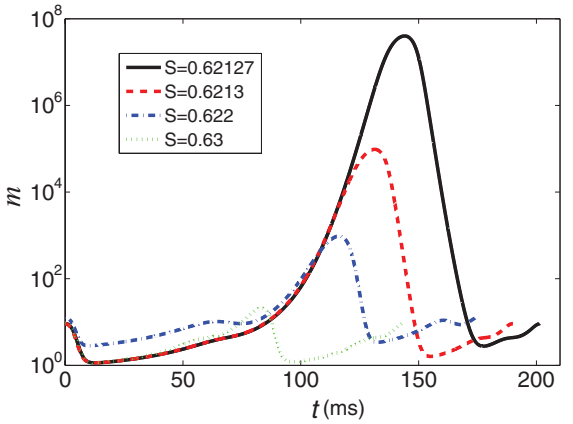

FIG. 10. (Color online) Stochastic sensitivity function $m(t)$ of limit cycles for the indicated values of S.

by the unlimited growth of the stochastic sensitivity toward the bifurcation point. The stochastic cloud around the equilibrium is then characterized by the confidence ellipse, Eq. (A4). The size of the confidence ellipse was determined by the noise strength (ε) and by the inherent dynamics, characterized by the eigenvalues of the stochastic sensitivity matrix, μ_1 and μ_2, shown in Fig. 7. Figure 8(a) shows the phase portrait of the deterministic system (1) along with a pseudoseparatrix dividing the zones of large-amplitude and small-amplitude trajectories in phase space. Here, the pseudoseparatrix is a particular phase curve geometrically delimiting these zones. The main results will not depend on the detailed choice of this phase curve. A similar approach to calculation of the pseudoseparatrix is discussed in [27].

In Fig. 8(b), an enlarged fragment of the phase portrait along with confidence ellipses is plotted. For small noise intensity $\varepsilon = 0.008$, the confidence ellipse is localized near the stable equilibrium in the subthreshold zone. In this case, the random trajectories oscillate with a small amplitude near the equilibrium (compare with the probability density function of Fig. 1, left panel). As the noise intensity increases, the confidence ellipses expands across the pseudoseparatrix and begins to occupy the suprathreshold zone [e.g., large ellipse in Fig. 8(b) for $\varepsilon = 0.015$]. This means that random

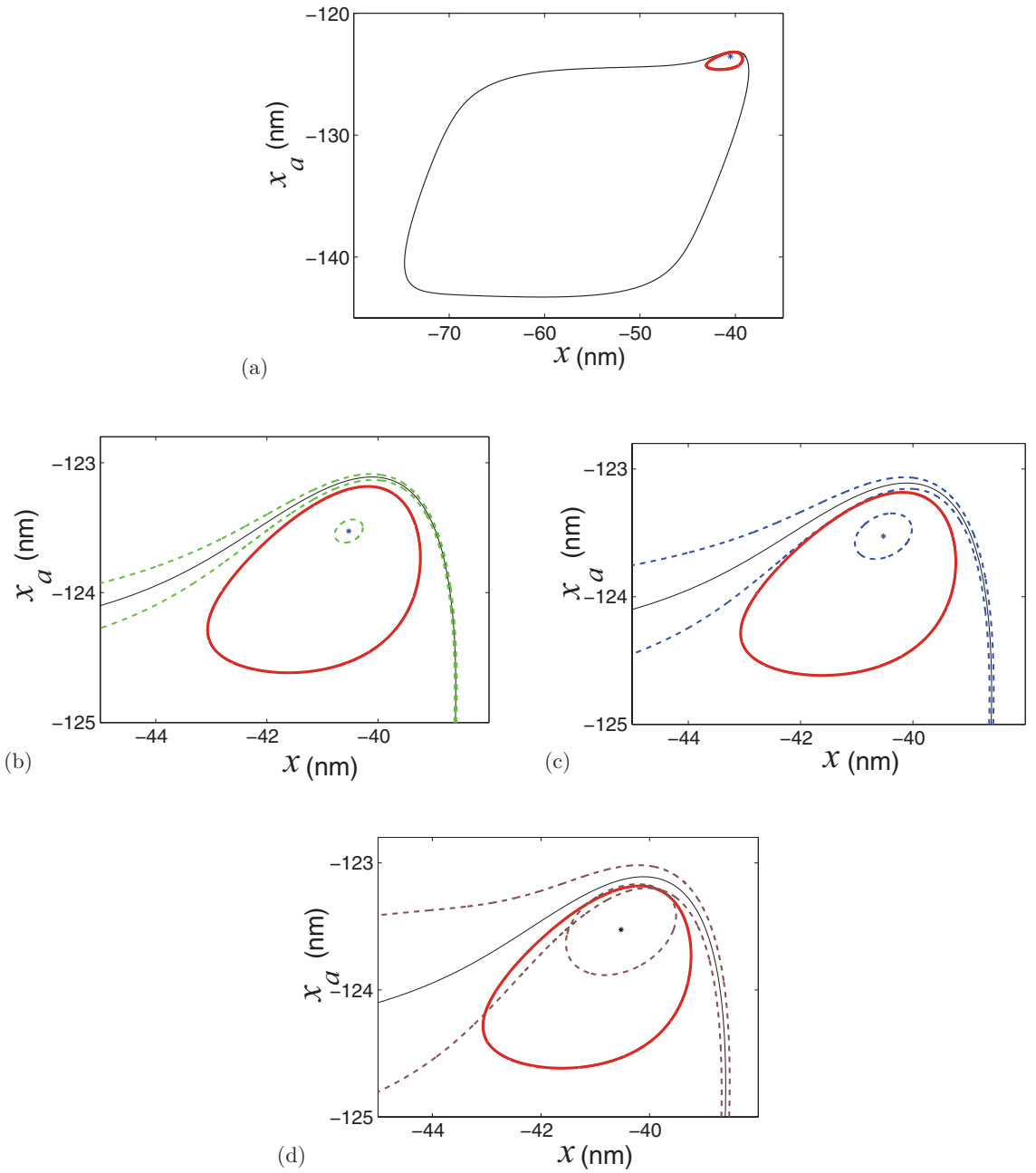

FIG. 11. (Color online) (a) Phase portrait for $S = 0.622$ with the stable limit cycle (black thin solid line), unstable cycle (red thick solid line), and stable equilibrium (asterisk). Confidence bands (dashed lines) for the fiducial probability $p = 0.999$ are shown for three noise intensities: (b) $\varepsilon = 0.002$ (green), (c) $\varepsilon = 0.004$ (blue), and (d) $\varepsilon = 0.008$ (brown).

trajectories of the forced system can exceed the boundary set by the pseudoseparatrix and proceed to large excursions with a high probability (see Fig. 1, middle and right panels). Figure 9 shows the distance d between confidence ellipses and the pseudoseparatrix versus noise intensity ε. The condition $d = 0$ marks the intersection of the ellipse with the pseudoseparatrix and thus sets up the threshold value of noise for the onset of large-amplitude excitations. The value $\varepsilon = 0.015$ is in agreement with the results obtained by direct numerical simulation (Fig. 3).

B. SSF analysis of bistability

Further we considered the parameter range $S_1 < S < S_2$ where the deterministic system (1) possesses a coexisting stable equilibrium and stable limit cycle. The basins of attraction of these stable states are separated by an unstable limit cycle. In the case of bistability the SSF analysis provides confidence domains for both attractors. The confidence domain for a stable limit cycle in two-dimensional (2D) phase space is represented by a confidence band whose size was determined by the stochastic sensitivity function $m(t)$ calculated along the limit cycle [Eq. (A5) in the Appendix]. Correspondingly, the confidence domain for the stable equilibrium is given by the ellipse as described in the previous section. Figure 10 shows the SSF, $m(t)$, for the stable limit cycle. The SSF is highly nonuniform along the limit cycle, elucidating parts of the periodic trajectory most susceptible to random perturbations. The maximum value of the SSF grows unlimitedly as the parameter S approaches the AH bifurcation value of $S_1 = 0.621269$.

Figure 11 shows mutual arrangements of coexisting attractors and corresponding confidence domains. For small noise, $\varepsilon = 0.002$, these domains (green dashed lines) do not cross the separatrix formed by the unstable limit cycle (red thick line) [see Fig. 11(b)]. In effect, random trajectories show small deviations from stable attractors (see, e.g., Fig. 4, left panel). So, the confidence domains adequately reflect the separation of corresponding random trajectories. For intermediate noise, $\varepsilon = 0.004$, the confidence band of the stable limit cycle (blue dashed line) crosses the separatrix while the confidence ellipse

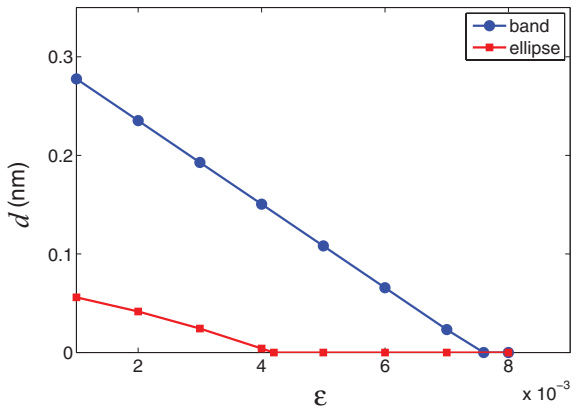

FIG. 12. (Color online) Minimal distance between the separatrix formed by the unstable cycle and confidence domains for $p = 0.999$ and $S = 0.622$: confidence ellipse of the stable equilibrium (blue line with circles); confidence band of the stable limit cycle (red line with squares).

of the stable equilibrium remains in its basin of the attraction [Fig. 11(c)]. This means that random trajectories start near the stable limit cycle, cross the separatrix, and remain near the equilibrium with high probability (Fig. 4, middle panel). Finally, for larger noise, $\varepsilon = 0.008$, both the confidence band of the stable limit cycle and the confidence ellipse of the equilibrium intersect the separatrix [Fig. 11(d)], resulting in frequent random hopping of phase trajectories between two basins of the attraction (Fig. 4, right panel).

To determine critical values of noise strength we again calculated the minimal distance, $d(\varepsilon)$, between the separatrix (unstable cycle) and confidence domains as functions of noise intensity ε, shown in Fig. 12. In agreement with direct numerical simulations (Fig. 6) the SSF method results in two critical noise values. The confidence band of the stable limit cycle touches the separatrix for $\varepsilon \approx 0.004$, indicating the first critical noise intensity. The confidence ellipse exceeds the separatrix for $\varepsilon \approx 0.008$, corresponding to the second critical noise intensity.

V. CONCLUSION

We applied an asymptotic method using the stochastic sensitivity function to study noise-induced effects near a subcritical Andronov-Hopf bifurcation in a biophysical model of a hair bundle. We considered the weak-noise limit, which distinguishes our study from other works on the so-called coherence resonance [19] in which noise was not weak as, e.g., in [23,47]. We have shown an interesting effect of noise-induced bifurcations in the regime of bistability of stable equilibrium and limit cycles. In the hair bundle model this resulted in stochastic oscillations with three distinct time scales: fast small-amplitude oscillations around the stable equilibrium, large-amplitude oscillations associated with the stable limit cycle, and slow noise-induced switching between those two oscillatory states. The last two regimes correspond to significant changes of the open probability of mechanoelectrical transduction ion channels and result in significant variations of the transduction current. Interestingly, the coherence of oscillations drops abruptly at the critical noise intensity, demonstrating a sort of coherence antiresonance, as Fig. 6 indicates. Such noise-induced transitions are hard to detect and characterize using direct numerical simulations without prior knowledge of the sensitivity of attractors to random perturbations. In the model these effects were observed for a rather weak noise, i.e., about two to three orders of magnitude smaller than realistic thermal noise in a *single* hair bundle [42]. We note, however, that noise is effectively reduced for coupled hair bundles [43–45]. In particular, for strong coupling the noise strength ε scales with the number of bundles, N, as $\varepsilon = 1/N^2$ [44], which makes it possible to observe multimodal oscillations in an experiment with $N = 10$–100 coupled hair bundles operating near subcritical AH bifurcation. We demonstrated how the stochastic sensitivity function method is used to understand the stochastic dynamics and to predict the critical noise intensity at which noise-induced transitions are most likely to occur. An obvious advantage of this method is that it does not rely on simulations of random trajectories, while it is indeed limited to weak noise perturbation. We stress that the SSF method is readily applicable to higher dimensional

models with multiplicative noise. For example, the stochastic Hodgkin-Huxley model with ion channel noise [41] can be studied with the SSF method, provided a large number of ion channels are present in a patch.

ACKNOWLEDGMENTS

This work was partially supported by the Ministry of Education and Science of Russia (Grant No. 1.1099.2011) and RFBR (Grant No. 13-08-00069).

APPENDIX: STOCHASTIC SENSITIVITY AND CONFIDENCE DOMAINS

Consider a general nonlinear deterministic system

$$\dot{x} = f(x). \tag{A1}$$

Here, x is an n vector, and $f(x)$ is an n vector function. It is supposed that the system (A1) has an exponentially stable attractor. For analysis of the effects of random external disturbances, we use a correspondent system of stochastic differential equations:

$$\dot{x} = f(x) + \varepsilon\sigma(x)\dot{w}. \tag{A2}$$

Here, $w(t)$ is an n-dimensional Wiener process and $\sigma(x)$ is an $n \times n$ matrix-valued function of the disturbances with intensity ε.

Random trajectories of the forced system (A2) leave a deterministic attractor and form a corresponding stochastic attractor with stationary probability distribution $\rho(x,\varepsilon)$, which is a stationary solution of the corresponding Fokker-Planck equation. In general, such a solution is hard or impossible to obtain. For weak-noise, asymptotics based on the quasipotential $v(x) = -\lim_{\varepsilon\to 0}\varepsilon^2 \log\rho(x,\varepsilon)$ are commonly used [34,35]. For small noise, one can write an approximation of $\rho(x,\varepsilon)$ as follows:

$$\rho(x,\varepsilon) \approx K\exp\left(-\frac{v(x)}{\varepsilon^2}\right).$$

At first, we consider stochastically forced equilibria. Let the system (A1) have an exponentially stable equilibrium $\bar{x}$. Under random disturbances stochastic states of the forced system (A2) concentrate around $\bar{x}$ and form a corresponding stochastic equilibrium with the stationary probabilistic distribution. In this case, the following quadratic approximation of the quasipotential $v(x) \approx \frac{1}{2}[x-\bar{x}, V(x-\bar{x})]$ is known. Here V is a positive definite $n \times n$ matrix. It allows an asymptotic of the stationary distribution in the Gaussian form

$$\rho(x,\varepsilon) \approx K\exp\left(-\frac{[x-\bar{x}, W^{-1}(x-\bar{x})]}{2\varepsilon^2}\right)$$

with the covariance matrix $\varepsilon^2 W$, where $W = V^{-1}$. For the exponentially stable equilibrium $\bar{x}$, the matrix W is a unique solution of the matrix equation

$$FW + WF^{\top} = -Q, \quad F = \frac{\partial f}{\partial x}(\bar{x}), \qquad Q = GG^{\top}, \quad G = \sigma(\bar{x}). \tag{A3}$$

The matrix W is a *stochastic sensitivity function* of the equilibrium $\bar{x}$. This matrix characterizes a spatial arrangement and size of the stationary distributed random states of the stochastic system (A2) around the deterministic equilibrium $\bar{x}$. Using this matrix, one can construct confidence domains for the geometrical description of the stochastic attractors.

For the 2D case, a confidence ellipse can be given by the following equation:

$$(x-\bar{x}, W^{-1}(x-\bar{x})) = 2k^2\varepsilon^2, \tag{A4}$$

where ε is the noise intensity, $k^2 = -\ln(1-p)$, and p is the fiducial probability. Let μ_1,μ_2 be eigenvalues and u_1,u_2 be normalized eigenvectors of the stochastic sensitivity matrix W. For the coordinates $z_1 = (x-\bar{x},u_1), z_2 = (x-\bar{x},u_2)$, the equation of the confidence ellipse can be written in standard form as

$$\frac{z_1^2}{\mu_1} + \frac{z_2^2}{\mu_2} = 2k^2\varepsilon^2.$$

Now consider a case when the system (A1) has an exponentially stable limit cycle corresponding to the T-periodic solution $x = \xi(t)$. Let Π_t be a hyperplane orthogonal to the cycle at the point $\xi(t)$ $(0 \leqslant t < T)$. In this case, for the Poincaré section Π_t in the neighborhood of the point $\xi(t)$ the quadratic approximation of the quasipotential is the following: $v(x) \approx \frac{1}{2}\{x-\xi(t), W^{+}(t)[x-\xi(t)]\}$. The corresponding Gaussian approximation of the stationary probabilistic distribution can be written as

$$\rho_t(x,\varepsilon) \approx K\exp\left(-\frac{[x-\xi(t)]^{\top}W^{+}(t)[x-\xi(t)]}{2\varepsilon^2}\right).$$

Here the stochastic sensitivity matrix $W(t)$ of the cycle is a unique solution [37] of the Lyapunov equation

$$\dot{W} = F(t)W + WF^{\top}(t) + P(t)Q(t)P(t)$$

with conditions

$$W(0) = W(T), \quad W(t)r(t) \equiv 0,$$

where $F(t) = \frac{\partial f}{\partial x}[\xi(t)]$, $Q(t) = \sigma(\xi(t))\sigma^{\top}(\xi(t))$, $r(t) = f(\xi(t))$, and $P(t)$ is a matrix of the orthogonal projection onto the hyperplane Π_t.

For the case $n = 2$, the stochastic sensitivity matrix $W(t)$ can be written as $W(t) = m(t)P(t)$. Here, $m(t) > 0$ is a T-periodic scalar stochastic sensitivity function satisfying the following boundary problem [36]:

$$\dot{m} = a(t)m + b(t), \quad m(0) = m(T) \tag{A5}$$

with T-periodic coefficients

$$a(t) = u^{\top}(t)[F^{\top}(t) + F(t)]u(t), \quad b(t) = u^{\top}(t)S(t)u(t),$$

where $u(t)$ is a normalized vector orthogonal to $f(\xi(t))$. The explicit solution $m(t)$ of the problem (A5) is given by

$$m(t) = g(t)[c + h(t)],$$

where

$$g(t) = \exp\left(\int_0^t a(s)ds\right), \quad h(t) = \int_0^t \frac{b(s)}{g(s)}ds, \qquad c = \frac{g(T)h(T)}{1-g(T)}.$$

The value $M = \max m(t), t \in [0,T]$, plays an important role in the analysis of stochastic dynamics near the limit cycle.

We shall consider M as a *stochastic sensitivity factor* of the cycle.

The stochastic sensitivity function $m(t)$ allows us to construct a confidence band around the deterministic cycle. For the line Π_t that is orthogonal to the cycle at the point $\xi(t)$, the corresponding confidence interval is given by the following equation:

$$[x - \xi(t)]^2 = 2k^2\varepsilon^2 m(t).$$

Hence, the boundaries $x_{1,2}(t)$ of the confidence band can be written in the explicit parametrical form

$$x_{1,2}(t) = \xi(t) \pm k\varepsilon\sqrt{2m(t)}u(t). \tag{A6}$$

Here the parameter k is connected with the fiducial probability p by the formula $k = \mathrm{erf}^{-1}(p)$, where $\mathrm{erf}(x) = \frac{2}{\sqrt{\pi}}\int_0^x e^{-t^2}dt$ is the error function.

[1] F. Moss and P. McClintock, *Noise in Nonlinear Dynamical Systems*, Vol. 1 (Cambridge University Press, Cambridge, England, 1989).

[2] V. Anishchenko, V. Astakhov, A. Neiman, T. Vadivasova, and L. Schimansky-Geier, *Nonlinear Dynamics of Chaotic and Stochastic Systems: Tutorial and Modern Developments*, Vol. 10 (Springer, New York, 2007).

[3] W. Horsthemke and R. Lefever, *Noise-Induced Transitions: Theory and Applications in Physics, Chemistry, and Biology*, Vol. 15 (Springer, New York, 2007).

[4] P. Landa and P. McClintock, Phys. Rep. **323**, 1 (2000).

[5] L. Arnold, *Random Dynamical Systems*, Vol. 2 (Springer, Berlin, 1998).

[6] R. Lefever and J. W. Turner, Phys. Rev. Lett. **56**, 1631 (1986).

[7] K. Mallick and P. Marcq, Eur. Phys. J. B **36**, 119 (2003).

[8] L. Gammaitoni, P. Hänggi, P. Jung, and F. Marchesoni, Rev. Mod. Phys. **70**, 223 (1998).

[9] M. McDonnell, N. Stocks, C. Pearce, and D. Abbott, *Stochastic Resonance: From Suprathreshold Stochastic Resonance to Stochastic Signal Quantization* (Cambridge University Press, Cambridge, England, 2008).

[10] V. Anishchenko, A. Neiman, F. Moss, and L. Shimansky-Geier, Phys.-Usp. **42**, 7 (1999).

[11] J. B. Gao, S. K. Hwang, and J. M. Liu, Phys. Rev. Lett. **82**, 1132 (1999).

[12] S. Ellner and P. Turchin, Oikos **111**, 620 (2005).

[13] Y. Lai and T. Tél, *Transient Chaos: Complex Dynamics on Finite Time Scales*, Vol. 173 (Springer, New York, 2011).

[14] B. Lindner, J. García-Ojalvo, A. Neiman, and L. Schimansky-Geier, Phys. Rep. **392**, 321 (2004).

[15] R. Kuske, L. F. Gordillo, and P. Greenwood, J. Theor. Biol. **245**, 459 (2007).

[16] R. J. Reategui and A. N. Pisarchik, Phys. Rev. E **69**, 067203 (2004).

[17] S. Aumaître, K. Mallick, and F. Pétrélis, J. Stat. Mech.: Theory Exp. (2007) P07016.

[18] M. Pradas, D. Tseluiko, S. Kalliadasis, D. T. Papageorgiou, and G. A. Pavliotis, Phys. Rev. Lett. **106**, 60602 (2011).

[19] A. S. Pikovsky and J. Kurths, Phys. Rev. Lett. **78**, 775 (1997).

[20] J. B. Gao, W.-W. Tung, and N. Rao, Phys. Rev. Lett. **89**, 254101 (2002).

[21] P. Borowski, R. Kuske, Y.-X. Li, and J. L. Cabrera, Chaos **20**, 043117 (2010).

[22] C. B. Muratov and E. Vanden-Eijnden, Chaos **18**, 015111 (2008).

[23] O. V. Ushakov, H.-J. Wünsche, F. Henneberger, I. A. Khovanov, L. Schimansky-Geier, and M. A. Zaks, Phys. Rev. Lett. **95**, 123903 (2005).

[24] C. Meunier and A. Verga, J. Stat. Phys. **50**, 345 (1988).

[25] A. J. Homburg and T. R. Young, Topol. Methods Nonlinear Anal. **35**, 77 (2010).

[26] S. Kraut, U. Feudel, and C. Grebogi, Phys. Rev. E **59**, 5253 (1999).

[27] N. Berglund and D. Landon, Nonlinearity **25**, 2303 (2012).

[28] R. E.Lee DeVille, E. Vanden-Eijnden, and C. B. Muratov, Phys. Rev. E **72**, 031105 (2005).

[29] C. Muratov *et al.*, Physica D (Amseterdam, Neth.) **210**, 227 (2005).

[30] H. Risken, *The Fokker-Planck Equation: Methods of Solution and Applications*, Vol. 18 (Springer Verlag, New York, 1996).

[31] R. Kuske, J. Stat. Phys. **96**, 797 (1999).

[32] R. Kuske and S. M. Baer, Bull. Math. Biol. **64**, 447 (2002).

[33] N. Berglund, B. Gentz, and C. Kuehn, J. Differ. Equations **252**, 4786 (2012).

[34] M. I. Freidlin and A. D. Wentzell, *Random Perturbations of Dynamical Systems*, Vol. 260 (Springer Verlag, New York, 1998).

[35] A. Dembo and O. Zeitouni, *Large Deviations Techniques and Applications*, Vol. 38 (Springer, New York, 2009).

[36] I. Bashkirtseva and L. Ryashko, Physica A (Amsterdam, Neth.) **278**, 126 (2000).

[37] I. Bashkirtseva and L. Ryashko, Math. Comput. Simul. **66**, 55 (2004).

[38] I. Bashkirtseva, L. Ryashko, and P. Stikhin, Fluctuation Noise Lett. **9**, 89 (2010).

[39] I. Bashkirtseva and L. Ryashko, Phys. Rev. E **83**, 061109 (2011).

[40] I. Bashkirtseva, G. Chen, and L. Ryashko, Chaos **22**, 033104 (2012).

[41] P. Rowat, Neural Comput. **19**, 1215 (2007).

[42] B. Nadrowski, P. Martin, and F. Jülicher, Proc. Natl. Acad. Sci. USA **101**, 12195 (2004).

[43] K. Dierkes, B. Lindner, and F. Jülicher, Proc. Natl. Acad. Sci. USA **105**, 18669 (2008).

[44] B. Lindner, K. Dierkes, and F. Jülicher, Phys. Rev. Lett. **103**, 250601 (2009).

[45] K. Dierkes, F. Jülicher, and B. Lindner, Eur. Phys. J. E Soft Matter **35**, 37 (2012).

[46] D. Clausznitzer, B. Lindner, F. Jülicher, and P. Martin, Phys. Rev. E: Stat., Nonlinear, Soft Matter Phys. **77**, 041901 (2008).

[47] W.-J. Rappel and S. Strogatz, Phys. Rev. E: Stat. Phys., Plasmas, Fluids, Relat. Interdiscip. Top. **50**, 3249 (1994).